The Astrophysical Journal Letters, 843:L2 (6pp), 2017 July 1 https://doi.org/10.3847/2041-8213/aa78f7

Searching for Interstellar C_{60}^+ Using a New Method for High Signal-to-noise *HST*/STIS Spectroscopy

M. A. Cordiner[1,2], N. L. J. Cox[3,4], R. Lallement[5], F. Najarro[6], J. Cami[7,8], T. R. Gull[1], B. H. Foing[9], H. Linnartz[10], D. J. Lindler[1,11], C. R. Proffitt[12], P. J. Sarre[13], and S. B. Charnley[1]

[1] NASA Goddard Space Flight Center, 8800 Greenbelt Road, Greenbelt, MD 20771, USA; martin.cordiner@nasa.gov
[2] Department of Physics, Catholic University of America, Washington, DC 20064, USA
[3] Anton Pannekoek Institute for Astronomy, University of Amsterdam, NL-1090 GE Amsterdam, The Netherlands
[4] Université de Toulouse, UPS-OMP, IRAP, F-31028, Toulouse, France
[5] GEPI, UMR8111, Observatoire de Paris, 5 Place Jules Janssen, F-92195, Meudon, France
[6] Departamento de Astrofísica, Centro de Astrobiología (CSIC/INTA), ctra. de Ajalvir km. 4, E-28850 Torrejón de Ardoz, Madrid, Spain
[7] Department of Physics and Astronomy and Centre for Planetary Science and Exploration (CPSX), The University of Western Ontario, London, ON N6A 3K7, Canada
[8] SETI Institute, 189 Bernardo Avenue, Suite 100, Mountain View, CA 94043, USA
[9] ESA ESTEC SCI-S, Noordwijk, The Netherlands
[10] Sackler Laboratory for Astrophysics, Leiden Observatory, Leiden University, P.O. Box 9513, NL 2300 RA Leiden, The Netherlands
[11] Sigma Space Corporation, 4600 Forbes Boulevard, Lanham, MD 20706, USA
[12] Space Telescope Science Institute, 3700 San Martin Drive, Baltimore, MD 21218, USA
[13] School of Chemistry, The University of Nottingham, University Park, Nottingham, NG7 2RD, UK
Received 2017 April 7; revised 2017 June 2; accepted 2017 June 6; published 2017 June 23

Abstract

Due to recent advances in laboratory spectroscopy, the first optical detection of a very large molecule has been claimed in the diffuse interstellar medium (ISM): C_{60}^+ (ionized Buckminsterfullerene). Confirming the presence of this molecule would have significant implications regarding the carbon budget and chemical complexity of the ISM. Here we present results from a new method for ultra-high signal-to-noise ratio (S/N) spectroscopy of background stars in the near-infrared (at wavelengths of 0.9–1 μm), using the *Hubble Space Telescope* (*HST*) Imaging Spectrograph (STIS) in a previously untested "STIS scan" mode. The use of *HST* provides the crucial benefit of eliminating the need for error-prone telluric-correction methods in the part of the spectrum where the C_{60}^+ bands lie and where the terrestrial water vapor contamination is severe. Our STIS spectrum of the heavily reddened B0 supergiant star BD+63 1964 reaches an unprecedented S/N for this instrument (~600–800), allowing the detection of the diffuse interstellar band (DIB) at 9577 Å attributed to C_{60}^+, as well as new DIBs in the near-IR. Unfortunately, the presence of overlapping stellar lines, and the unexpected weakness of the C_{60}^+ bands in this sightline, prevents conclusive detection of the weaker C_{60}^+ bands. A probable correlation between the 9577 Å DIB strength and interstellar radiation field is identified, which suggests that more strongly irradiated interstellar sightlines will provide the optimal targets for future C_{60}^+ searches.

Key words: instrumentation: spectrographs – ISM: molecules – line: identification – techniques: spectroscopic

1. Introduction

The diffuse interstellar band (DIB) problem is the longest-standing puzzle in interstellar chemistry, seemingly impenetrable despite the dedicated efforts of astronomers and laboratory chemists since the early 20th century (Herbig 1995; Sarre 2006; Snow 2014). The DIBs manifest as broad spectroscopic absorption features in the optical to near-infrared (NIR) spectra of stars as their light passes through the diffuse interstellar medium (ISM), indicating the presence of a large quantity of (mostly carbonaceous) unidentified molecular material (e.g., Cordiner 2011). Foing & Ehrenfreund (1994) discovered two DIBs at 9577 Å and 9632 Å that they assigned to C_{60}^+ (ionized Buckminsterfullerene) based on a similarity with the absorption wavelengths that are seen in neon matrix spectroscopy (d'Hendecourt et al. 1992; Fulara et al. 1993). Recently obtained gas-phase spectra of C_{60}^+–He_n complexes (for $n \leqslant 4$; Campbell et al. 2015, 2016a; Kuhn et al. 2016) show that the match between the interstellar and laboratory wavelengths is accurate within the observational uncertainties (a fraction of an angström). The bare C_{60}^+ absorption wavelengths were confirmed in an independent laboratory study by Spieler et al. (2017) using C_{60}^+ cations embedded in He-droplets.

If confirmed, the detection of interstellar C_{60}^+ will constitute a major breakthrough in interstellar chemistry and may provide, for the first time, an insight into the true scale of the chemical complexity in the diffuse ISM. Measurements of the NIR electronic transitions of C_{60}^+ (in absorption) would also provide a unique complement to the discovery of mid-infrared C_{60} and C_{60}^+ emission bands in circumstellar and interstellar environments (Cami et al. 2010; Sellgren et al. 2010; Berné et al. 2013).

Despite dedicated observational studies (Walker et al. 2015, 2016; Galazutdinov et al. 2017), the case for interstellar C_{60}^+ has not yet been proven beyond reasonable doubt. Based on the laboratory measurements, five absorption features are expected (at 9348.4, 9365.2, 9427.8, 9577.0, and 9632.1 Å, with strength ratios 0.07:0.2:0.3:1.0:0.8; Campbell et al. 2016b). Galazutdinov et al. (2017) were unable to confirm the presence of the weakest 3 features in a sample of 19 heavily reddened Galactic sightlines observed from the ground. Instead of a constant ratio for the two strongest C_{60}^+ DIBs (λ9577 and λ9632), as expected for electronic transitions arising from a $^2A_{1u}$ ground vibronic state, Galazutdinov et al. (2017) found that the interstellar band ratio was highly variable among different lines of sight. We note, however, that if the observed

transitions involve lower levels above the ground state (such as the split levels arising from Jahn–Teller distortion), a variable ratio could potentially occur. Although Walker et al. (2016) claimed interstellar detections of all five C_{60}^+ bands, the three weaker C_{60}^+ bands are problematic as they fall in a wavelength region heavily obscured by absorption due to water vapor in the Earth's atmosphere (see Galazutdinov et al. 2000, 2017). Telluric-correction methods for such weak interstellar absorption features are error-prone as a result of incomplete telluric line cancelation, and from the possible presence of weak (unseen) stellar lines in the telluric standard spectrum. To rigorously confirm the identification of interstellar C_{60}^+, high signal-to-noise observations of all five absorption bands are required, preferably from outside Earth's atmosphere.

In this Letter, we present the first ever ultra-high signal-to-noise ratio (S/N), high resolution stellar/interstellar spectra obtained using the *Hubble Space Telescope* (*HST*) imaging spectrograph, targeting four of the five C_{60}^+ features (λ9349, λ9365, λ9428, and λ9577) along a heavily reddened line of sight. Very high continuum signal-to-noise ratios (S/N > 500 per spectral channel) are commonly achieved using ground-based optical telescopes, but such sensitivity has not previously been obtained using (direct) *HST* spectroscopy at red and near-IR wavelengths due to severe CCD fringing. After successfully employing a previously untested "STIS scan" observing mode to trail the target star along the spectrograph slit (crossing hundreds of CCD rows to facilitate fringe cancelation), unprecedented S/Ns ∼ 600–800 per dispersion pixel have been obtained. These spectra have permitted the first search for weak interstellar absorption features in the NIR, unhindered by telluric absorption.

2. Observations and Data Reduction

To reliably detect the weaker C_{60}^+ DIBs, a high-S/N interstellar spectrum is required with minimal contamination from interloping stellar photospheric lines. The heavily reddened ($E_{B-V} = 1.01$) B0 I star BD+63 1964 was selected due to its extremely strong DIBs—the majority of DIBs are among the strongest for stars of comparable extinction (Tuairisg et al. 2000)—as well as its early spectral type and relatively clean predicted spectrum in the vicinity of the λ9365 and λ9428 C_{60}^+ bands. The lightly reddened B0 I star 69 Cygni ($E_{B-V} = 0.14$) was selected for comparison, to assist in the discrimination of stellar and interstellar features.

2.1. HST/STIS

Data were acquired over a single orbit for 69 Cyg and two orbits for BD+63 1964 using the G750M grating with a central wavelength of 9336 Å (covering the range 9050–9610 Å). This covers four of the five known C_{60}^+ bands; a change of grating tilt would be required to obtain the fifth band. We used the $52'' \times 0.''1$ slit, and the plate scale was $0.''05$ per pixel. Following peakup and focusing maneuvers, a series of STIS-scan exposures was performed for each star, trailing the star along the slit at a constant rate with the shutter held open. For 69 Cyg, six exposures were obtained: two long scans spanning up to 1000 detector rows and four shorter scans spanning ∼300 rows. The scan direction was alternated for successive exposures. For BD+63 1964 (observed in a separate visit after the optimal observing sequence had been established), eight identical forward scans were obtained spanning 700 detector rows each, toward the upper part of the CCD. A pair of flat-field exposures (contemporaneous fringe flats) was obtained in sequence following each pair of target star exposures, and 5–6 additional pairs of flats were obtained to fill in the remaining orbital time during occultation. Exposures of a Pt/Cr–Ne lamp were obtained during each orbit for wavelength calibration. Subsequent conversion from vacuum to air wavelengths was performed using the Morton (2000) formula.

The STIS CCD suffers from charge transfer inefficiency (CTI) during readout, as a result of long-term radiation damage. The raw frames were corrected for CTI using the procedure outlined by Anderson & Bedin (2010)[14], which significantly reduces the severity of bad CCD columns. Standard dark current, bias, geometric distortion, and wavelength corrections were performed using the IRAF `calstis` package (Hodge et al. 1998). For BD+63 1964, the four trailed science exposures in each orbit were sufficiently well matched to allow statistical cosmic-ray rejection using `ocrreject`. This was not possible for 69 Cyg due to imperfect registration of the exposed rows between each frame, which may have occurred due to errors in the guide star tracking, as well as possible exposure timing errors.

Spectral extraction was performed by summing the counts along CCD columns. Bad pixels and residual cosmic rays were rejected based on their standard deviation (using a 3σ threshold), after normalizing the individual CCD rows by their median levels. Such row normalization was required due to variations in the illumination function along the slit, resulting from slight variations in the slit width and telescope scan rate. Scattered-light subtraction was performed with a low-order fit to the light under the two occulting bars (positioned 1/3 and 2/3 of the way along the slit). Extracted Pt/Cr–Ne lamp line widths were consistent with the nominal instrumental resolving power of 10,000 (30 km s^{-1}).

The STIS CCD suffers from severe fringing due to internal reflections at wavelengths greater than 700 nm, where the chip starts to become transparent to incoming light. Fringe amplitudes are variable with wavelength, with a maximum of ±20% near 900 nm (see, e.g., Figure 1). The aim of our fringe cancelation strategy was to match as closely as possible the illumination pattern of the science exposure to that of the flat field by STIS scanning. This approach has the major advantages of (1) reducing the impact of individual bad pixels and cosmic-ray hits, (2) allowing for orders of magnitude increases in the number of counts per science exposure, and (3) eliminating the need to change the slit mechanism during observations, resulting in a consistent optical setup for the science and flat-field exposures.

As shown in Figure 1, scanning the exposed star across hundreds of CCD rows results in significantly reduced fringe amplitudes (a five-fold reduction in the spectral rms in this case). Following correction using a contemporaneous fringe flat, we obtained apparently complete fringe cancelation down to the level of the statistical noise.

2.2. CFHT ESPaDOnS

For comparison with our STIS data, four 1000 s exposures of BD+63 1964 were obtained over two nights in 2016 December, using the ESPaDOnS échelle spectrograph of the

[14] See http://www.stsci.edu/hst/stis/software/analyzing/scripts/pixel_based_CTI.

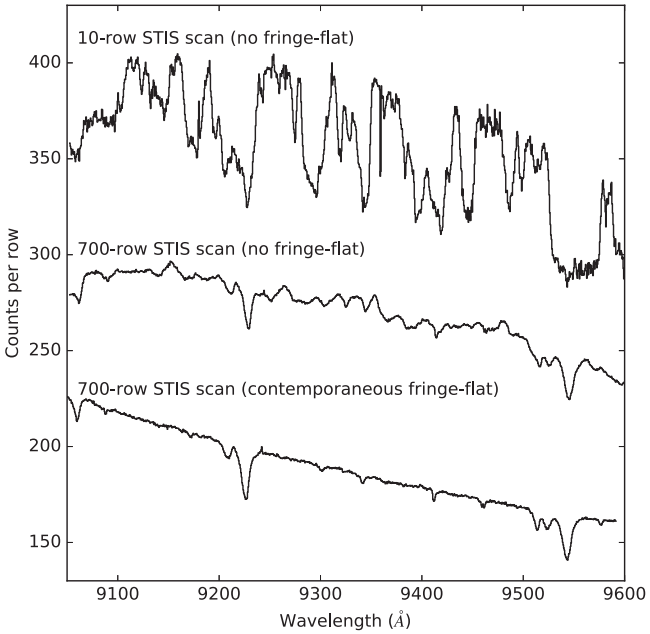

Figure 1. *HST* spectra of BD+63 1964 using three different scanning/flat-fielding schemes (with additive vertical offsets). Top: standard STIS spectroscopic acquisition and reduction (extracted over 10 dispersion rows), showing severe CCD fringing. Middle: a substantial reduction in fringe amplitude is achieved by STIS scanning (extracted over 700 dispersion rows). Bottom: the combined result of STIS scanning and flat fielding using a contemporaneous (in-orbit) fringe flat.

Canada–France–Hawaii Telescope (CFHT). Observing conditions were good and the airmass was in the range of 1.41–1.49. The data were reduced by the automated Upena pipeline, which uses the Libre-ESpRIT data reduction software (Donati et al. 1997). The reduced spectra cover the range 370–1048 nm at a resolving power of ∼80,000, and have a continuum signal-to-noise ratio of ∼500 at 900 nm.

Due to the forest of atmospheric H_2O absorption lines in our STIS range, the ESPaDOnS spectra need to be telluric-corrected. The conventional approach of division by a standard star is unreliable for the measurement of weak DIBs due to the likely presence of stellar features in the standard star spectrum, which would introduce artifacts upon division. We therefore adopted a transmission modeling approach, using synthetic atmospheric transmittances provided by the TAPAS website[15] (Bertaux et al. 2014), adapted for Mauna Kea. A preliminary telluric correction was performed using the "rope length" method for weak to moderately strong lines (Raimond et al. 2012), excluding from the length the spectral intervals corresponding to the central parts of the strongest lines. The preliminary correction was then interpolated in the most heavily contaminated intervals to remove residual artifacts. Next, the observed data were fitted to the convolved product of this spectrum and the TAPAS synthetic transmittance, allowing for variable airmass, refined wavelength correction, and variable line-spread function. The observed data were divided by this new adjusted transmission spectrum to provide a new corrected spectrum. The second step was then iterated to convergence to produce the final corrected spectrum. Despite our best efforts, telluric residuals still remain at the locations of the most heavily saturated lines, which may be due to the time variability of the telluric spectrum, scattered-light residuals, or small asymmetries in the ESPaDOnS instrumental response function.

[15] http://ether.ipsl.jussieu.fr/tapas/

2.3. Comparison between STIS and ESPaDOnS Spectra

The main purpose of these ESPaDOnS spectra was to verify the reliability of our nonstandard STIS observation and reduction procedures. A comparison between the *HST*/STIS and the telluric-corrected CFHT/ESPaDOnS spectra is shown in Figure 2. Telluric-correction artifacts in panels (a) and (b) are severe, preventing a reliable comparison in the vicinity of the weaker C_{60}^+ bands. However, in the less problematic range 9500–9600 Å (panel (c)), the agreement between the two instruments is excellent, which demonstrates the success of our STIS observation and data reduction strategy. Slight discrepancies may be due to differences in the instrumental resolving power, telluric-correction residuals, or uncertainties in the continuum level of the high-dispersion CFHT spectrum. Some uncertainty in the STIS scattered-light correction also remains, leading to uncertainty in the zero level. A more detailed characterization of the (2D) scattered-light properties for STIS scan exposures awaits further study.

3. Results

The combined scattered-light-subtracted exposures of BD +63 1964 and 69 Cyg reached total counts of 8×10^5 and 5.5×10^5, respectively (per dispersion pixel). The presence of weak stellar and interstellar features precludes an accurate measurement of the continuum rms, but in regions free of any obvious lines, S/N = 600–800 was found for BD+63 1964 and ∼700 for 69 Cyg. To our knowledge, this is the highest S/N ever demonstrated with STIS for direct near-infrared spectroscopy at full grating resolution. The continuum-normalized spectra are shown in Figure 3.

Both stars are B0 supergiants and have nearly identical stellar spectra. We used the non-LTE model atmosphere code CMFGEN (Hillier & Miller 1998, 1999; Hillier 2011), which solves the radiative-transfer equation for a spherically symmetric wind in the comoving frame under the constraints of radiative and statistical equilibrium. An effective temperature of 27,000 K, macro-turbulent velocity of 120 km s^{-1}, and projected rotational velocity of 85 km s^{-1} were derived for both of the stars. The modeled lines are identified in Figure 3. Four features stand out in the BD+63 1964 spectrum that are not present in 69 Cyg or in the stellar model, which are likely due to interstellar absorption. The first three of these (at 9088, 9302, and 9412 Å) are identified as new DIBs; Galazutdinov et al. (2000) also found a possible DIB near 9412 Å. The absorption feature at 9577 Å coincides with the laboratory C_{60}^+ wavelength. 69 Cyg also shows evidence for weak absorptions at 9577 and 9412 Å.

The equivalent width (EW) of the λ9577 band is 74 ± 3 mÅ. A Gaussian fit to its profile gives EW = 76 ± 3 mÅ, with a central wavelength of 9576.60 ± 0.03 Å, a central depth of 2.3%, and FWHM = 3.1 ± 0.1 Å. These line strength measurements may be considered accurate to within about ±10% due to uncertainties in the STIS scattered-light subtraction.

A close-up view of the four observed C_{60}^+ band regions is shown in Figure 4. A spectral model for C_{60}^+ is overlaid using the laboratory wavelengths and band strengths of Campbell et al. (2016a). We adopt Gaussian band shapes because a

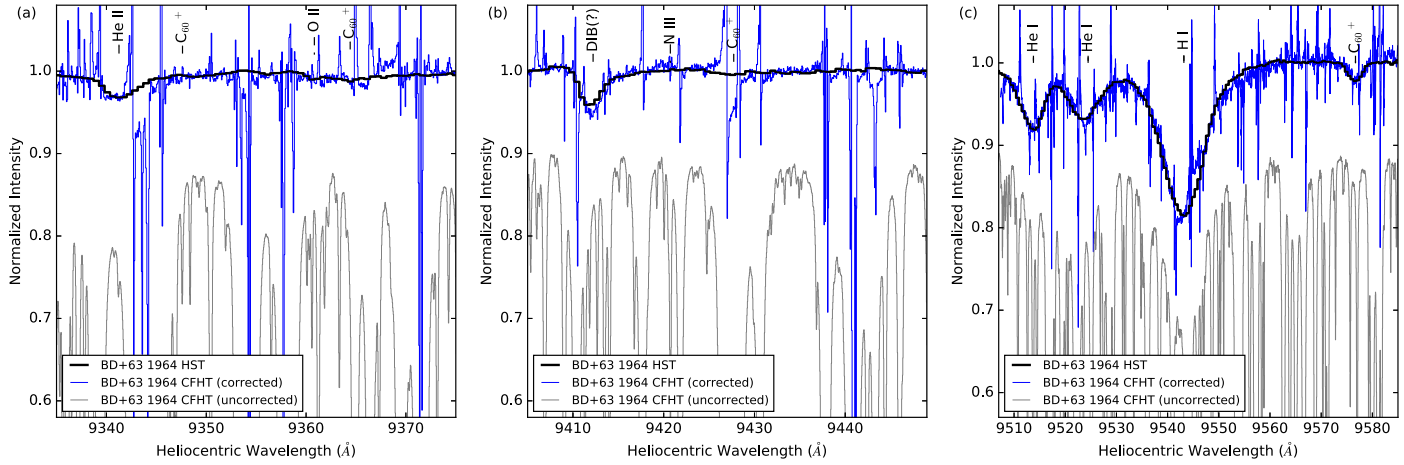

Figure 2. Comparison of *HST*/STIS and CFHT/ESPaDOnS spectra of BD+63 1964, normalized with a linear continuum. CFHT spectra were telluric-corrected using a TAPAS model; the uncorrected CFHT spectra (dominated by telluric absorption) are shown in gray with a vertical offset of −0.1. Artifacts in the corrected CFHT spectra are primarily due to incomplete cancelation around the strongest telluric lines. The match between the strengths of the H and He lines in panel (c) demonstrates close consistency of the STIS and ESPaDOnS calibrations.

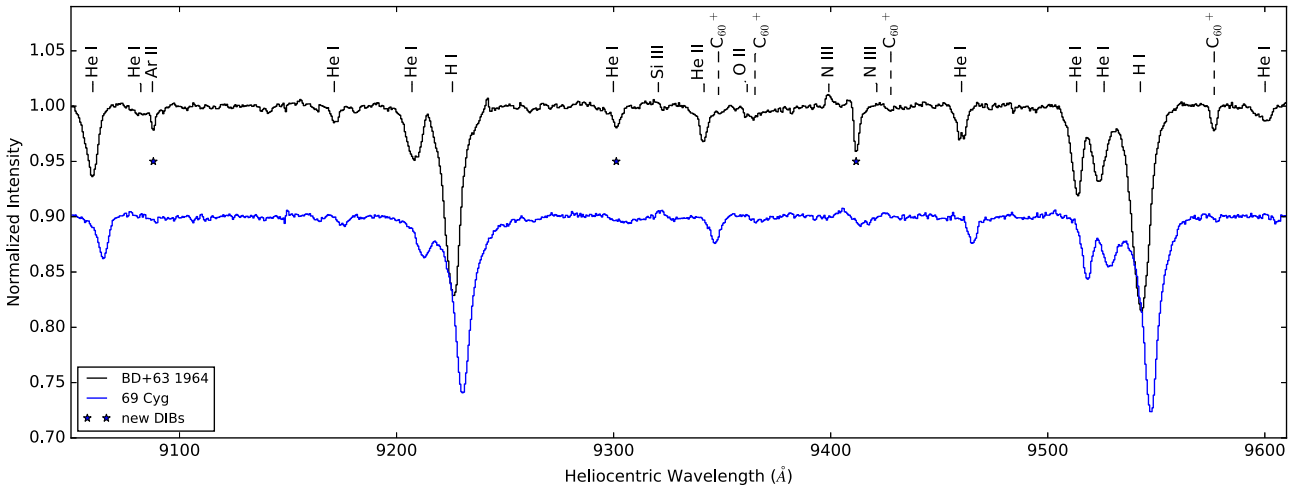

Figure 3. STIS NIR spectra of BD+63 1964 and 69 Cyg (offset vertically for display). Stellar features (in the rest frame of BD+63 1964) and the positions of the laboratory C_{60}^+ bands (in the interstellar rest frame) are labeled. Possible new DIBs are marked with asterisks.

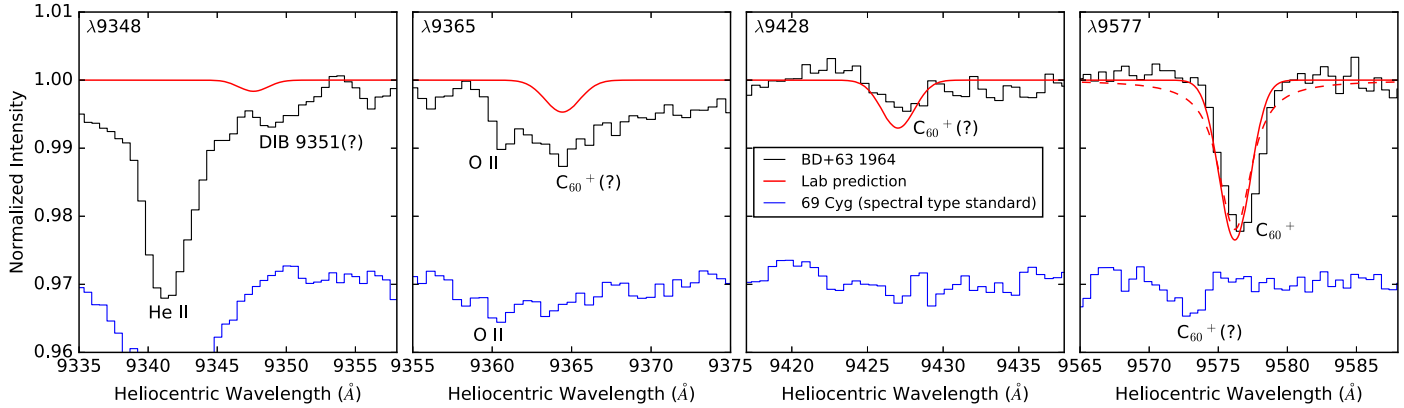

Figure 4. STIS NIR spectra of BD+63 1964 (black histograms) and the spectral-type standard 69 Cyg (blue histograms; shifted in wavelength to align the stellar features and offset vertically for display) for the four C_{60}^+ bands in our spectral range. The red curves show predicted C_{60}^+ DIB profiles based on Campbell et al. (2016b), Doppler-shifted to match the radial velocity of interstellar K I toward BD+63 1964. A Lorentzian model profile is also shown for λ9577 (dashed line). Detected and tentative (?) stellar and interstellar features are labeled.

Lorentzian profile provides a poor match for the observed λ9577 band wings (Figure 4). The model has been Doppler shifted to match the interstellar K I velocity. As with most heavily reddened diffuse sightlines, the K I line toward BD+63 1964 (recorded in our ESPaDOnS data) shows a complex velocity structure, with three main components at

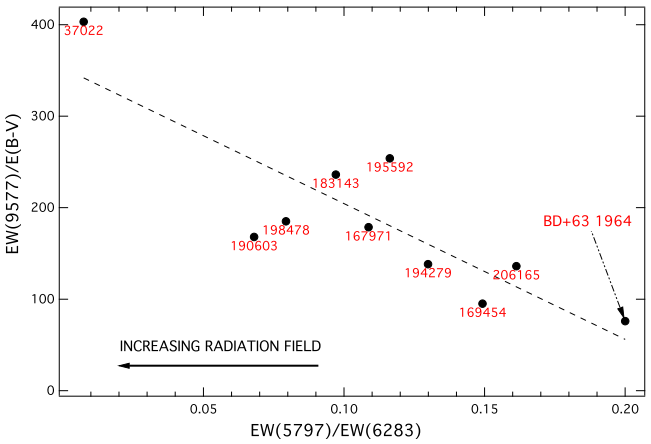

Figure 5. Strength of the λ9577 C_{60}^{+} band (per unit reddening) vs. the equivalent width ratio of the λ6283 and λ5797 DIBs (an indicator of radiation field strength) for a sample of Galactic sightlines, labeled by HD number.

-16, -27, and -33 km s^{-1}. We take the average of these (-25 km s^{-1}) as the interstellar C_{60}^{+} radial velocity. The λ9577 band carrier abundance could be variable across the three K I clouds (due to variations in chemical abundances and ionization levels), so we assign an error margin of ± 10 km s^{-1}, which corresponds to ± 0.3 Å. Within the uncertainties, our inferred (Doppler corrected) λ9577 rest wavelength of 9577.4 Å matches the laboratory value of 9577.0 $\pm$ 0.2 Å; the slight redshift could indicate that C_{60}^{+} is associated more with the higher-velocity K I gas. The 1.0 Å instrumental resolution contributes 0.2 Å to the observed DIB FWHM. The additional (0.4 Å) of broadening in the observed band compared with the laboratory measurement of 2.5 Å is consistent with the spread of interstellar K I velocities in this sightline.

We find weak absorption features in our BD+63 1964 spectrum close to the wavelengths of the λ9348, λ9365, and λ9428 C_{60}^{+} bands. These features are not present toward our standard star 69 Cyg, and may therefore be due to interstellar C_{60}^{+}. However, the appearance of the λ9348 band is far from clear due to contamination by another possible weak DIB at 9350 Å (previously identified at a rest wavelength of 9351 Å by Walker et al. 2016), as well as overlapping stellar He II absorption. The λ9365 feature is partially contaminated by a weak stellar O II line, and is broader and deeper than expected. The λ9428 feature is too weak for a reliable measurement.

4. Discussion

The strengths of different DIBs are known to vary among sightlines with differing physical and chemical properties, independent of the total amount of interstellar material (e.g., Krełowski & Walker 1987; Ehrenfreund & Jenniskens 1995; Cami et al. 1997; Elyajouri et al. 2017; Ensor et al. 2017). The EW per unit reddening (EW/E_{B-V}) provides a measure of the relative strength of a given DIB. For BD+63 1964 we find EW(9577)/E_{B-V} = 73 mÅ, which is among the smallest values known for this band. Unfortunately for our present study, this means that BD+63 1964 is one of the least favorable heavily reddened sightlines in which to search for C_{60}^{+}, which explains to some degree our difficulties in establishing (or disproving) the presence of the weaker C_{60}^{+} absorption bands.

The extreme weakness of the λ9577 band per unit E_{B-V} may be due to a lower than normal degree of ionization in this sightline. The well-known DIB at 6283 Å has a large EW/E_{B-V} value in diffuse clouds that are strongly irradiated by UV (see above references), while the 5797 Å DIB tends to be favored in more neutral, less irradiated clouds. The λ5797/λ6283 EW ratio is thus considered to be a tracer of the radiation field strength in the line of sight. Data have been taken from compilations of optical DIB measurements by Xiang et al. (2017) and the λ9577 measurements of Galazutdinov et al. (2000) to study the relationship between EW(9577)/E_{B-V} and the λ5797/λ6283 DIB strength ratio. Additional λ6283 and λ5797 measurements were obtained from archival data from the CFHT and Telescope Bernard Lyot. The results for nine sightlines are shown in Figure 5, including the present results for BD+63 1964. Even without HD 37022 (a highly irradiated sightline through the Orion Nebula with unusually high EW(9577)/E_{B-V}), the trend is for increasing λ9577 strength in gas pervaded by stronger radiation fields. In a survey of DIBs and atomic lines toward BD+63 1964 by Ehrenfreund et al. (1997), a relatively high gas density and low level of ionization was inferred, and the extremely low λ5797/λ6283 ratio is suggestive of weakly irradiated gas. The trend for increasing EW(9577)/E_{B-V} with radiation field strength is consistent with the assignment to C_{60}^{+} or another species whose ionization stage becomes dominant in more irradiated diffuse clouds (see also Foing & Ehrenfreund 1997).

5. Conclusion

We performed the first successful test of the *HST* "STIS scan" spectroscopic observational mode. The resulting spectroscopic S/N (up to ~800) is, to our knowledge, by far the highest demonstrated with STIS for direct stellar measurements at full grating resolution. This technical demonstration opens up a new wavelength range for interstellar, stellar, and exoplanetary spectroscopy, with unprecedented sensitivity.

We obtained the first "clean" measurements of the spectral region covering the λ9348, λ9365, λ9428, and λ9577 C_{60}^{+} bands without the confounding presence of telluric contamination or fringing artifacts. The λ9577 band exhibits a closely Gaussian shape with FWHM and peak wavelength consistent with laboratory measurements. However, due to the surprising weakness of the C_{60}^{+} features in our chosen sightline, the strengths and profiles of the (intrinsically weaker) λ9348, λ9365, or λ9428 bands could not be reliably measured. We identify a correlation between the λ9577 band strength (per unit reddening) and the λ5797/λ6283 DIB strength ratio (an indicator for radiation field strength), which suggests that the weakness of λ9577 toward BD+63 1964 is due to a low-radiation environment, consistent with the assignment of this DIB to an ion of a species whose first ionization energy is much less than that of neutral hydrogen (13.6 eV), and whose second ionization energy is $\gtrsim$13.6 eV. Using the STIS scanning technique, high-S/N *HST* spectroscopy of more strongly UV-irradiated heavily reddened sightlines may provide the best opportunity for a conclusive identification of all five C_{60}^{+} bands, which will be required to place the detection of this molecule beyond reasonable doubt.

Possible new DIBs are reported at 9088, 9302, and 9412 Å. Their interstellar origin may be confirmed by follow-up studies of stars with differing spectral types and degrees of extinction.

Based on observations made with the NASA/ESA *Hubble Space Telescope* (program #14705). Support was provided by

NASA through a grant from the Space Telescope Science Institute, which is operated by the Association of Universities for Research in Astronomy, Inc., under NASA contract NAS 5-26555. F.N. acknowledges Spanish grants FIS2012-39162-C06-01, ESP2013-47809-C3-1-R, and ESP2015-65597-C4-1-R. ESPaDOnS observations were obtained under program 16BD86 at the Canada–France–Hawaii Telescope, which is operated by the National Research Council of Canada, the Institut National des Sciences de l'Univers of the Centre National de la Recherche Scientifique of France, and the University of Hawaii.

Facilities: HST (STIS), CFHT(ESPaDOnS).

References

Anderson, J., & Bedin, L. R. 2010, PASP, 122, 1035
Berné, O., Mulas, G., & Joblin, C. 2013, A&A Letters, 550, 4
Bertaux, J. L., Lallement, R., Ferron, S., Boonne, C., & Bodichon, R. 2014, A&A, 564, A46
Cami, J., Bernard-Salas, J., Peeters, E., & Malek, S. E. 2010, Sci, 329, 1180
Cami, J., Sonnentrucker, P., Ehrenfreund, P., & Foing, B. H. 1997, A&A, 326, 822
Campbell, E. K., Holz, M., Gerlich, D., & Maier, J. P. 2015, Natur, 523, 322
Campbell, E. K., Holz, M., Maier, J. P., et al. 2016a, ApJ, 822, 17
Campbell, E. K., Holz, M., & Maier, J. P. 2016b, ApJL, 826, L4
Cordiner, M. A. 2011, in Encyclopedia of Astrobiology (Berlin: Springer), 432
d'Hendecourt, L., Fostiropoulos, K., & Léger, A. 1992, PhD thesis, Univ. Paris VII
Donati, J.-F., Semel, M., Carter, B. D., et al. 1997, MNRAS, 291, 658
Ehrenfreund, P., Cami, J., Dartois, E., & Foing, B. H. 1997, A&A, 318, L28
Ehrenfreund, P., & Jenniskens, P. 1995, in The Diffuse Interstellar Bands, Astrophysics and Space Science Library, Vol. 202, ed. A. G. G. M. Tielens & T. P. Snow (Dordrecht: Kluwer Academic), 105
Elyajouri, M., Lallement, R., Monreal-Ibero, A., Capitanio, L., & Cox, N. L. J. 2017, A&A, 600, A129
Ensor, T., Cami, J., Bhatt, N. H., & Soddu, A. 2017, ApJ, 836, 162
Foing, B. H., & Ehrenfreund, P. 1994, Natur, 369, 296
Foing, B. H., & Ehrenfreund, P. 1997, A&A, 319, 59
Fulara, J., Jakobi, M., & Maier, J. P. 1993, CPL, 211, 227
Galazutdinov, G. A., Krełowski, J., Musaev, F. A., Ehrenfreund, P., & Foing, B. H. 2000, MNRAS, 317, 750
Galazutdinov, G. A., Shimansky, V. V., Bondar, A., Valyavin, G., & Krełowski, J. 2017, MNRAS, 465, 3956
Herbig, G. H. 1995, ARA&A, 33, 19
Hillier, D. J. 2011, APSS, 336, 87
Hillier, D. J., & Miller, D. L. 1998, ApJ, 496, 407
Hillier, D. J., & Miller, D. L. 1999, ApJ, 519, 354
Hodge, P. E., Hulbert, S. J., Lindler, D., et al. 1998, in ASP Conf. Ser. 145, Astronomical Data Analysis Software and Systems VII, ed. R. Albrecht, R. N. Hook, & H. A. Bushouse (San Francisco, CA: ASP), 316
Krełowski, J., & Walker, G. A. H. 1987, ApJ, 312, 860
Kuhn, M., Renzler, M., Postler, J., et al. 2016, NatCo, 7, 13550
Morton, D. C. 2000, ApJS, 130, 403
Raimond, S., Lallement, R., Vergely, J. L., Babusiaux, C., & Eyer, L. 2012, A&A, 544, A136
Sarre, P. J. 2006, JMoSp, 238, 1
Sellgren, K., Werner, M. W., Ingalls, J. G., et al. 2010, ApJL, 722, L54
Snow, T. P. 2014, IAUS, 297, 3
Spieler, S., Kuhn, M., Postler, J., et al. 2017, ApJ, submitted
Tuairisg, S. Ó., Cami, J., Foing, B. H., Sonnentrucker, P., & Ehrenfreund, P. 2000, A&AS, 142, 225
Walker, G. A. H., Bohlender, D. A., Maier, J. P., & Campbell, E. K. 2015, ApJL, 812, L8
Walker, G. A. H., Campbell, E. K., Maier, J. P., Bohlender, D., & Malo, L. 2016, ApJ, 831, 130
Xiang, F. Y., Li, Aigen., & Zhong, J. X. 2017, ApJ, 835, 107